Supplementary Information

A 10 ka ice core from Tödi (Switzerland) reveals recent surface loss and revises Alpine age–altitude relationships

Michelle M. Worek[1,2], David Wachs[3,4], Anja Eichler[1,2], Matthias Huss[5,6], Raphael Moser[5,6], Sabina Brütsch[1], Sönke Szidat[2,7], Margit Schwikowski[1,2,7], Theo M. Jenk[1,2]

[1]PSI Center for Energy and Environmental Sciences, Paul Scherrer Institute, Villigen, Switzerland
[2]Oeschger Centre for Climate Change Research, University of Bern, Bern, Switzerland
[3]Institute of Environmental Physics, Heidelberg University, Heidelberg, Germany
[4]Kirchhoff-Institute for Physics, Heidelberg University, Heidelberg, Germany
[5]Laboratory of Hydraulics, Hydrology and Glaciology, ETH Zürich, Zürich, Switzerland
[6]Swiss Federal Institute for Forest, Snow and Landscape Research, Birmensdorf, Switzerland
[7]Department of Chemistry, Biochemistry, and Pharmaceutical Sciences, University of Bern, Bern, Switzerland

S1. Topographic maps of Glarner Tödi

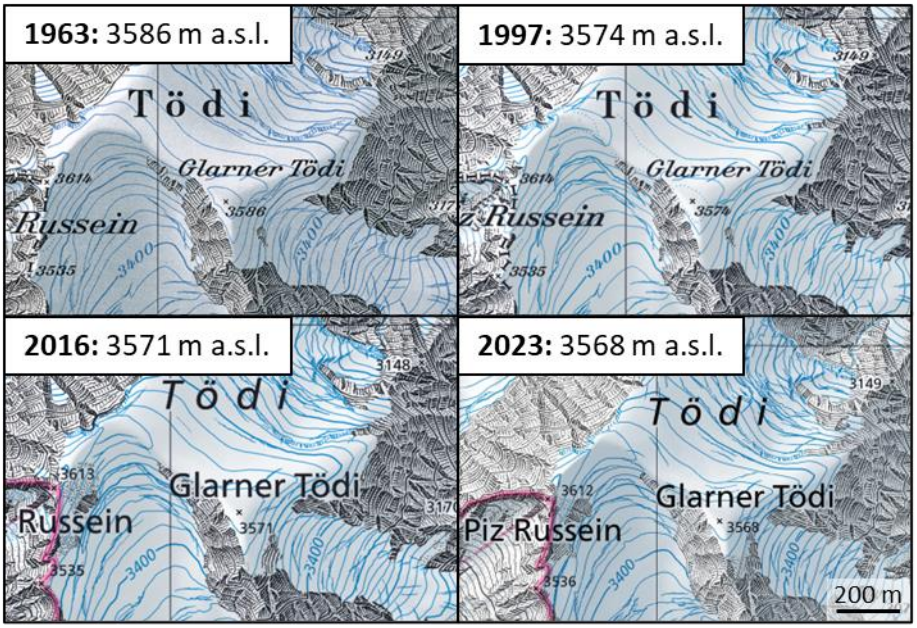

Figure S1. Historical maps of Tödi massif, Glarner Tödi elevation indicated (Federal Office of Topography, 1963, 1997, 2016, 2023).

S2. Basal ice core

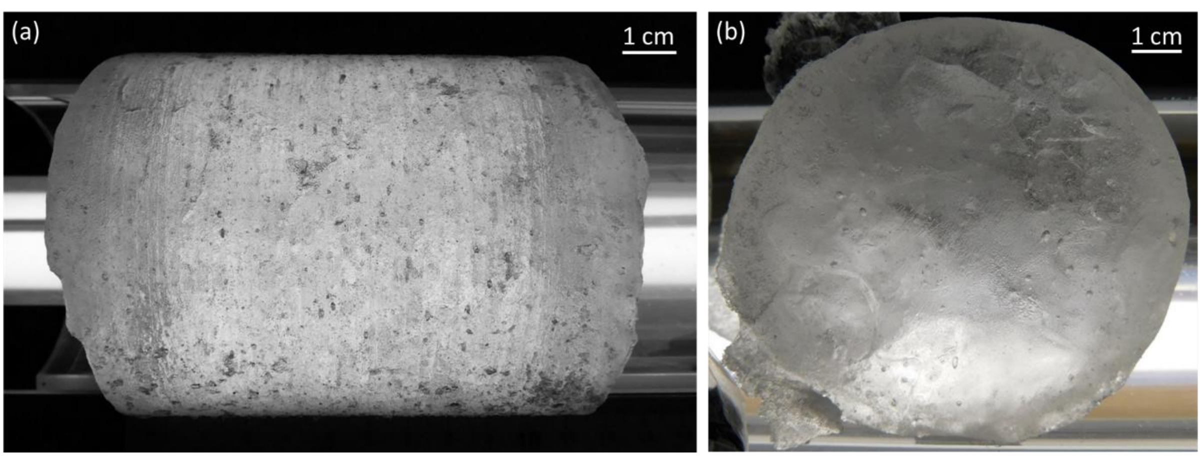

Figure S2. Basal ice core, (a) side view, with top direction of core to the left. (b) basal view, with smooth imprint of bedrock (fine lineations). Photos were taken in the PSI cold room during sample preparation in July 2024.

S3. Ground penetrating radar and modelling of winter mass balance

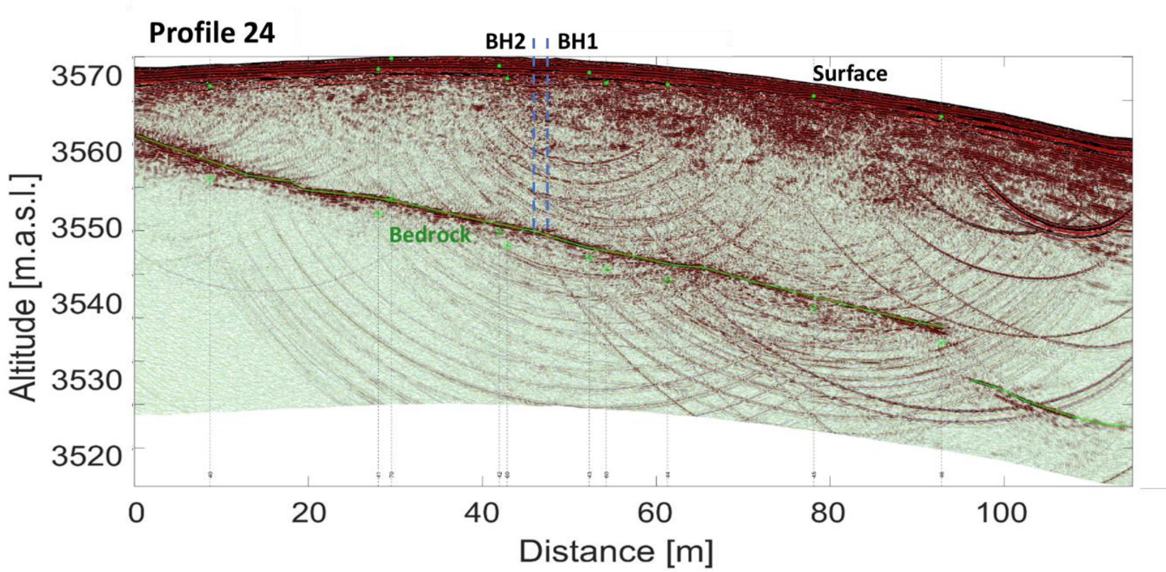

Figure S3. Profile 24 (west-east traverse of drill site, see Fig. 2). TÖ23-BH1 and TÖ23-BH2 are indicated, in addition to the surface (black) and the bedrock (green).

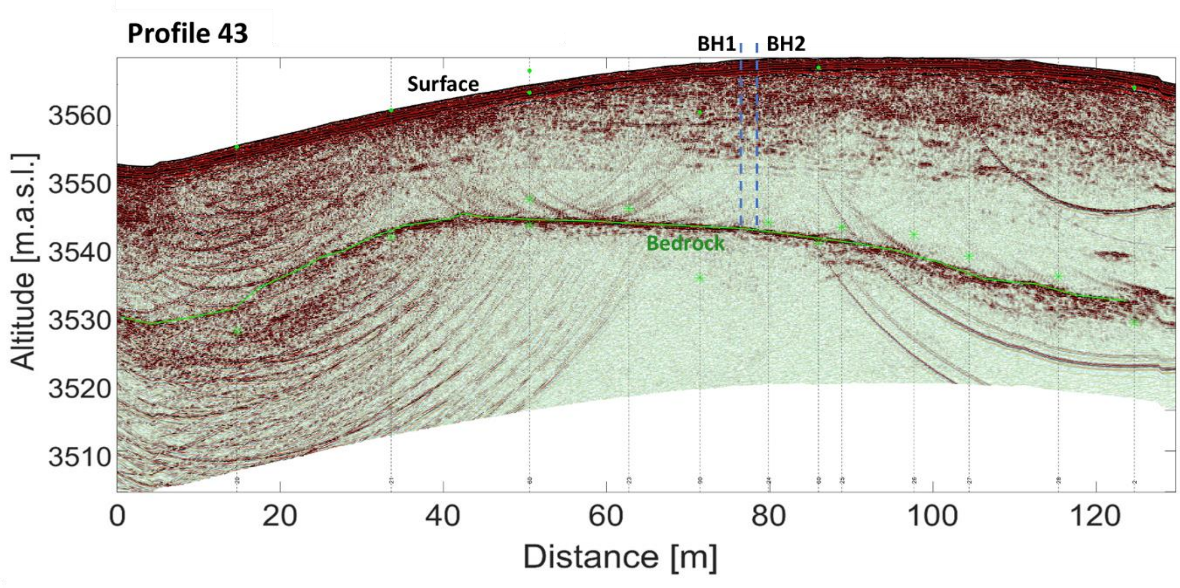

Figure S4. Profile 43 (north-south traverse of drill site, see Fig. 2). TÖ23-BH1 and TÖ23-BH2 are indicated, in addition to surface (black) and the bedrock (green).

Winter mass balance for the 2022–2023 period was close to zero at the summit (around 0.1 m w.e.), reflecting limited preservation of winter snowfall. Accumulation is spatially heterogeneous, with higher accumulation observed on the north–northeast slope, where the ice is thicker. This pattern is consistent with frequent high-wind conditions at the site, which promote snow redistribution and surface scouring.

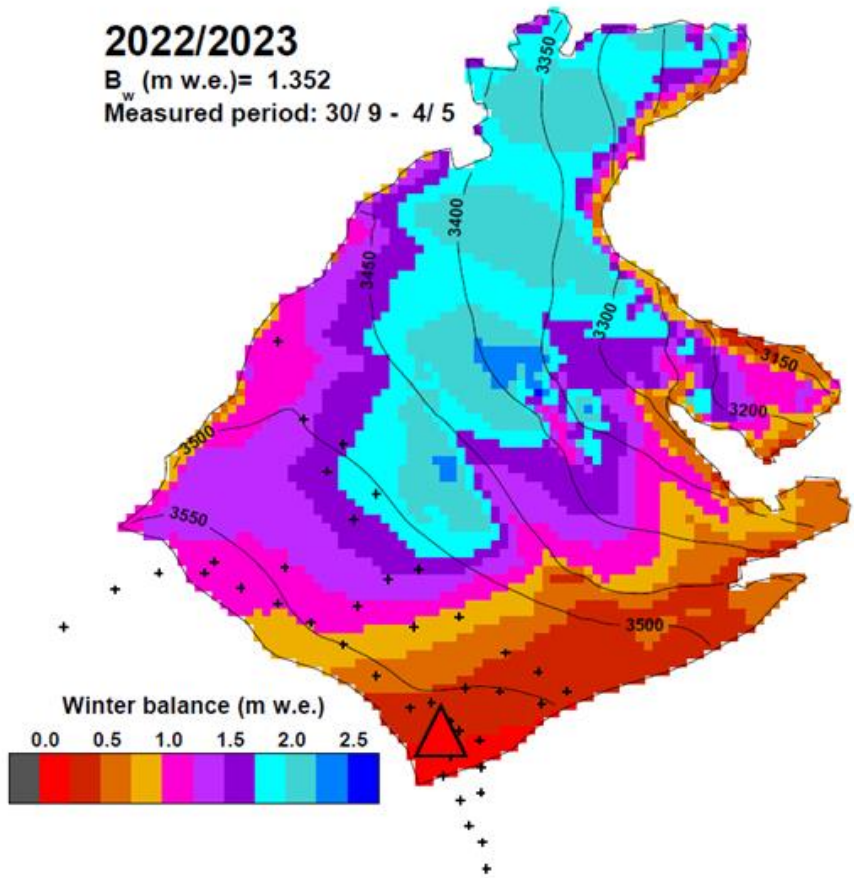

Figure S5. Spatial distribution from model-based extrapolation of the winter mass balance of Tödi glacier based on snow probing (black crosses). The red triangle indicates the drilling site. See Section 3.1 and 3.4.

S4. ^{210}Pb background correction

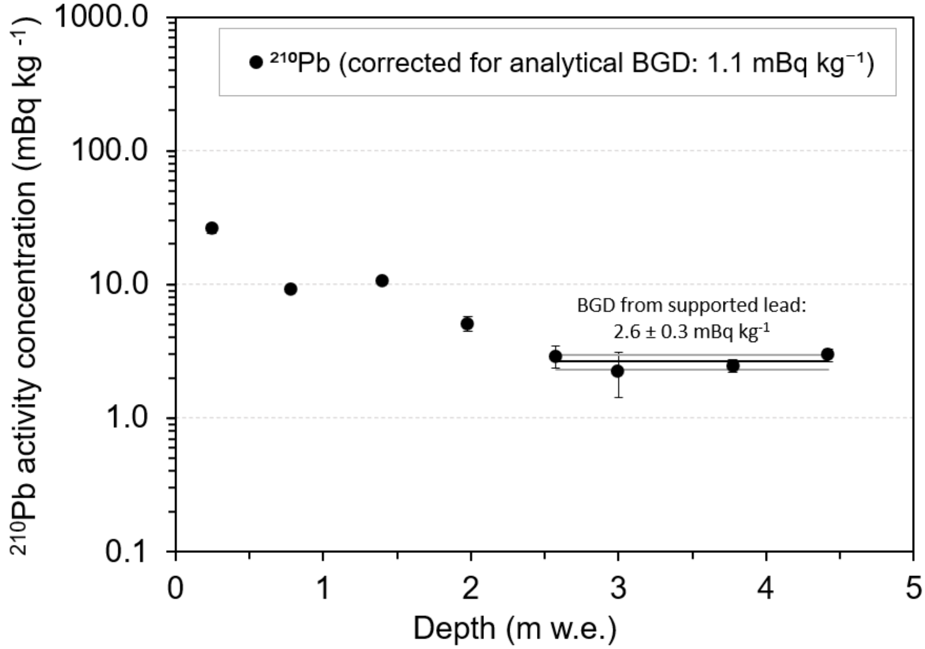

Figure S6. Plateau of ^{210}Pb activity concentration background from supported lead. Subsequently subtracted from the values of the four samples above, finally used for the ^{210}Pb dating. See Gäggeler et al. (2020) for further explanation.

S5. Ice flow modelling

S5.1 Dansgaard-Johnsen model

The Dansgaard-Johnsen **(**D–J) model assumes a non-uniform vertical strain-rate due to shear near the bed in case of cold ice frozen to bedrock (Dansgaard and Johnsen, 1969). This allows for stronger layer thinning close to bedrock, unlike the Nye model which assumes basal sliding (Nye, 1963). Thereby, the simple final model expression was derived by applying a close approximation of the horizontal velocity $w(z)$ as a function of depth, with the ice column of total thickness H being divided into an upper layer with constant velocity and a lower shear layer of thickness h with increased strain, resulting from $w(z)$ proportionally decreasing to zero at bedrock (for the same average annual accumulation rate, b, and H, and with $h = 0$, the D–J model derives the exact same solution as the Nye model). For the upper layer, if the distance above the bedrock (height above bedrock), z, is greater than or equal to the thickness of the shear layer, h, the modeled age, $t(z)$, is given by

$$t(z) = -\frac{2H-h}{2b} ln \frac{2z-h}{2H-h}, \quad h \le z < H \quad (1)$$

For the lower layer, if the distance above the bedrock, z, is less than the thickness of the shear layer, h, the modeled age, $t(z)$, is given by

$$t(z) = \frac{2H - h}{b}\left(\frac{h}{z} - 1\right) + t_h, \quad 0 \leq z \leq h \quad (2)$$

(t_h being the age of ice at $z = h$, given by Equation 1). This formulation allows for significantly older ice near the bed.

Derivation of solutions included minimization of the misfit between model age, t_m, and observed age t. For minimizing the misfit function, we followed the approach from Fahnestock et al. (2001) of time-weighted residual sum of squares, which accounts for lower (absolute) precision in the dating of older layers:

$$f(H, b, h) = \sum_{i=1}^{n}\left[\frac{t_m(i) - t(i)}{t(i)}\right]^2 \quad (3)$$

n being the number of observations. Solving was performed with a non-linear Generalized Reduced Gradient algorithm (with multi-start for tuned parameters).

S5.2 Coupling of the Dansgaard-Johnsen ice flow model with the firn densification model

For simplicity, considering overall uncertainties, we neglected the term for densification due to refreezing of meltwater in the firn densification model (see equation 5 in Huss, 2013). Coupling between the two models was achieved as follows:

initiating, H_0: to reduce number of iterations until conversion of values, the initial value of H if only available in units of m was multiplied by a density of 750 kg m^{-3} before input into the D-J model,

step 1: for pre-set (fixed) H_0, derivation of D-J model solutions for b, $t_m(z)$ and h - if not fixed - by misfit minimization to input $t(1, ..., n)$,

step 2: input of b and $t_m(z)$ into the densification model,

step 3: recalculation of H in m w.e. using the modelled densities with a maximum of 910 kg m^{-3} (H_1),

restart with step 1, until b and H converge to stable values.

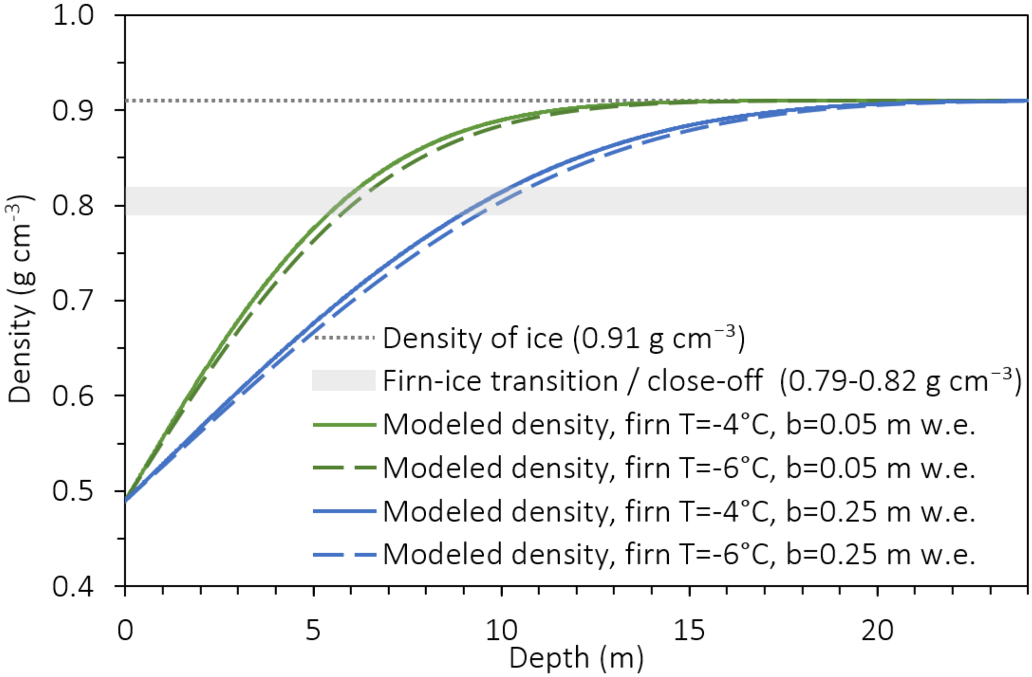

Figure S7. Modeled density profiles for Tödi based on the indicated parameter values for temperature, T, and annual accumulation rate, *b* (Huss, 2013). Also shown are typical densities for ice and for the firn-ice transition, which is roughly equivalent to the typical close-off depth (depth where the air in the ice is trapped in isolated pockets/bubbles; Schwander et al., 1988).

S6. ^{39}Ar dating - Δage correction

The trapping process of air in ice causes an age difference between the gas enclosed in air bubbles and the surrounding ice (Δage). The Δage is controlled by the time air spends in the diffusive firn column above bubble close-off (e.g., Buizert, 2021; Schwander et al., 1988). For alpine sites, only very limited information on Δage is available. So far, a value of around 30 years has typically been applied for ^{39}Ar dating of glacier ice (Hou et al., 2025; Ritterbusch et al., 2022; Wachs et al., 2026). Here, we estimate Δage from the residence time of air in the diffusive firn column above bubble close-off, also considering firn ventilation particularly relevant for sites of high wind exposure and relatively low firn column height. For Δage correction, we here assumed a physical firn column thickness between 15 to 20 m (see main text). Using the Herron–Langway densification model with a rate constant k = 1380 derived for Alpine sites (Huss, 2013) and for $T = -5°C$, this corresponds to a column thickness of around 11–16 m w.e. Because of ventilation, the wind driven, rapid exchange of air in the upper convective layer (typically the upper 2–3 m; i.e. around 1.1–1.8 m w.e.) and because the lock-in zone already occurs at densities of ~790–820 kg m^{-3} (Schwander et al., 1988), in our case at ~6–10 m depth (see Figure S7 corresponding to ~3.5–6.5 m w.e.), the effective diffusive column length (L_d) is reduced to approximately:

$$L_d \approx 2 - 5\, m\, w.e.$$

Using the fundamental relationship between Δage and L_d (Buizert, 2021) and an accumulation rate of 0.1-0.3 m w.e. a^{-1} (b, see main text) yields:

$$\Delta age = \frac{L_d}{b} = \frac{3.5 \pm 1.5\, m\, w.e}{0.2\ \pm\ 0.1\, m\, w.e.a^{-1}} \approx 18 \pm 12\, a$$

This value likely still represents an upper estimate of Δage, because processes such as melt–refreeze can increase densification rates and form ice layers that partially seal off air at shallower depths. Both effects reduce L_d and consequentially the Δage.

S7. Basal age compilation

Table S1. Basal age compilation. *DDG basal age based on $\delta^{18}O$ wiggle matching with other records, not ^{14}C.

Site	Surface Elevation (m a.s.l.)	Ice Thickness / Borehole Depth (m)	Bedrock Elevation (m a.s.l.)	Basal ^{14}C Age (ka cal BP)	Reference
Tödi	3565	20	3545	~10	This study
WSS	3500	10	3490	~6	(Bohleber et al., 2020)
CG	4455	~80	4375	~15.2 (lower limit)	(Jenk et al., 2009; Sigl et al., 2009)
CDD	4250	124	4126	~5	(Preunkert et al., 2019)
DDG	4304	40	4264	~12*	(Legrand et al., 2025)
Ortles	3859	75	3784	~7	(Gabrielli et al., 2016; Gabrielli et al., 2026)

Table S2. ^{14}C ages used in Figure 11. For sample depths only reported in m, ice density in these lowermost ice core sections is assumed to be 910 kg m^{-3}.

Site	Height above bed (m w.e.)	Calibrated Age (years b2k)	σ
Tödi	8.46	307	85
	7.81	420	51
	6.76	471	51
	5.58	524	45
	4.48	625	47
	3.84	821	66
	3.26	947	94
	2.68	1088	85
	2.16	1250	80
	1.75	1495	83
	1.33	2460	123
	0.90	3073	124
	0.63	4383	158
	0.46	6457	123
	0.40	7457	154
	0.22	9287	187
	0.09	10017	367
WSS	5.48	673	350
	4.50	785	145
	2.82	1397	456
	1.24	2240	104
	0.73	3711	200
	0.38	5934	739
	0.09	14070	332
DDG	9.96	2129	2013
	8.58	1152	821
	7.32	1164	262
	6.78	1190	308
	5.79	2221	616
	5.21	2002	398
	4.35	2855	269
	3.25	4996	540
	2.32	6436	492
	1.45	8493	343
	1.20	9458	410
CG	11.12	441	330
	10.26	647	214
	9.035	884	238
	8.1	1149	242
	6.04	1501	329
	4.48	1949	395
	2.51	2514	472
	1.95	3612	400
	1.37	4044	382
	0.81	8722	1425
	0.34	15197	
Ortles	5.91	639	204
	2.72	1558	288
	2.30	2232	126
	1.68	2659	102
	0.86	4221	524
	0.64	5226	531
	0.44	6789	364
CDD	4.65	461	320
	3.54	1760	695
	2.52	867	524
	1.72	1548	434
	0.67	2288	337
	0.12	5071	597

S8. Difference in determined accumulation rates for Tödi and WSS

While differences in accumulation patterns may be due to topographic factors such as summit prominence and wind exposure (Tödi has a prominence of 1570 m compared to ~340 m for WSS), here, we discuss the differences in methodological approaches for deriving accumulation rates on Tödi and WSS. For one, the WSS 2019 ice core only covers around 20% of the past ice thickness. This imposes a serious challenge for the modelling needed for the derivation of the mean annual accumulation rate. Further, different models were used, the D–J model for Tödi and the 2-parameter model from Bolzan (1985), in which the parameter determining the strain rate is related to glacier geometry which is difficult to assess and less intuitive than the parameter for the shear zone height h in the D–J model for which boundaries are clearly defined with $H \geq h \geq 0$; considering the requirement of incompressibility below the depth of the firn–ice transition (H_{FIT}; at around 0.8* H) by $H_{FIT} \geq h \geq 0$ (see Gabrielli et al., 2026). Further, in this study, we accounted for the density of the lost surface. The largest effect may however be related to the selection of the reference year. While for model input, we maintain the date of layers according to the ages determined based on the law of radioactive decay for ^{210}Pb, ^{39}Ar and ^{14}C (as age before sampling and analysis), in the WSS modeling approach around 100 years were subtracted to be consistent with the (reference) date of last steady-state conditions in ice thickness (1914 CE), the thickness used as model input. In the modelling context, this does not consider a gradual loss of mass over time and assumes an immediate stop of the ice flow with no further thinning of the remaining layers. We believe that the approach presented in this study is more consistent with the underlying fundamentals. A back of the envelope calculation with our modelling approach for the reported, uncorrected ages and an ice thickness of 47 m (~40 m w.e.) results in a 30-40% lower estimate of the accumulation rate (b = ~0.2-0.4 m w.e. a^{-1}) than previously suggested.

References

Bohleber, P., Schwikowski, M., Stocker-Waldhuber, M., Fang, L., and Fischer, A.: New glacier evidence for ice-free summits during the life of the Tyrolean Iceman, Scientific Reports, 10, 20513, 2020.

Bolzan, J. F.: Ice flow at the Dome C ice divide based on a deep temperature profile, Journal of Geophysical Research: Atmospheres, 90, 8111-8124, 1985.

Buizert, C.: The Ice Core Gas Age-Ice Age Difference as a Proxy for Surface Temperature, Geophysical Research Letters, 48, e2021GL094241, 2021.

Dansgaard, W. and Johnsen, S. J.: A Flow Model and a Time Scale for the Ice Core from Camp Century, Greenland, Journal of Glaciology, 8, 215-223, 1969.

Fahnestock, M., Abdalati, W., Luo, S., and Gogineni, S.: Internal layer tracing and age-depth-accumulation relationships for the northern Greenland ice sheet, Journal of Geophysical Research: Atmospheres, 106, 33789-33797, 2001.

Federal Office of Topography, swisstopo: Tödi, Blatt 1193, Landeskarte der Schweiz 1:25,000, Federal Office of Topography swisstopo, Wabern, Switzerland, 1963.

Federal Office of Topography, swisstopo: Tödi, Blatt 1193, Landeskarte der Schweiz 1:25,000, Federal Office of Topography swisstopo, Wabern, Switzerland, 1997.

Federal Office of Topography, swisstopo: Tödi, Blatt 1193, Landeskarte der Schweiz 1:25,000, Federal Office of Topography swisstopo, Wabern, Switzerland, 2016.

Federal Office of Topography, swisstopo: Tödi, Blatt 1193, Landeskarte der Schweiz 1:25,000, Federal Office of Topography swisstopo, Wabern, Switzerland, 2023.

Gabrielli, P., Barbante, C., Bertagna, G., Bertó, M., Binder, D., Carton, A., Carturan, L., Cazorzi, F., Cozzi, G., Dalla Fontana, G., Davis, M., De Blasi, F., Dinale, R., Dragà, G., Dreossi, G., Festi, D., Frezzotti, M., Gabrieli, J., Galos, S. P., Ginot, P., Heidenwolf, P., Jenk, T. M., Kehrwald, N., Kenny, D., Magand, O., Mair, V., Mikhalenko, V., Lin, P. N., Oeggl, K., Piffer, G., Rinaldi, M., Schotterer, U., Schwikowski, M., Seppi, R., Spolaor, A., Stenni, B., Tonidandel, D., Uglietti, C., Zagorodnov, V., Zanoner, T., and Zennaro, P.: Age of the Mt. Ortles ice cores, the Tyrolean Iceman and glaciation of the highest summit of South Tyrol since the Northern Hemisphere Climatic Optimum, The Cryosphere, 10, 2779-2797, 2016.

Gabrielli, P., Jenk, T. M., Bertó, M., Dreossi, G., Festi, D., Kofler, W., Winstrup, M., Oeggl, K., Schwikowski, M., Stenni, B., and Barbante, C.: A multimillennial Alpine ice core chronology synchronized with an accurately dated Arctic Pb record, EGUsphere, 2026, 1-24, 2026.

Gäggeler, H. W., Tobler, L., Schwikowski, M., and Jenk, T. M.: Application of the radionuclide 210Pb in glaciology – an overview, Journal of Glaciology, 66, 447-456, 2020.

Hou, S., Jenk, T. M., Jiang, W., Zhang, W., Hu, H., Feng, X., Li, H., Wu, S.-Y., Pang, H., Yu, J., Huang, R., Lu, Z.-T., Yang, G.-M., Bender, M., and Schwikowski, M.: A radiometric timescale challenges the chronology of the iconic 1992 Guliya ice core, Science Advances, 11, eadx8837, 2025.

Huss, M.: Density assumptions for converting geodetic glacier volume change to mass change, The Cryosphere, 7, 877-887, 2013.

Jenk, T. M., Szidat, S., Bolius, D., Sigl, M., Gäggeler, H. W., Wacker, L., Ruff, M., Barbante, C., Boutron, C. F., and Schwikowski, M.: A novel radiocarbon dating technique applied to an ice core from the Alps indicating late Pleistocene ages, Journal of Geophysical Research: Atmospheres, 114, 2009.

Legrand, M., McConnell, J. R., Preunkert, S., Wachs, D., Chellman, N. J., Rehfeld, K., Bergametti, G., Wensman, S. M., Aeschbach, W., Oberthaler, M. K., and Friedrich, R.: Alpine ice core record of large changes in dust, sea-salt, and biogenic aerosol over Europe during deglaciation, PNAS Nexus, 4, 2025.

Nye, J. F.: On the Theory of the Advance and Retreat of Glaciers, Geophysical Journal International, 7, 431-456, 1963.

Preunkert, S., McConnell, J. R., Hoffmann, H., Legrand, M., Wilson, A. I., Eckhardt, S., Stohl, A., Chellman, N. J., Arienzo, M. M., and Friedrich, R.: Lead and Antimony in Basal Ice From Col du Dome (French Alps) Dated With Radiocarbon: A Record of Pollution During Antiquity, Geophysical Research Letters, 46, 4953-4961, 2019.

Ritterbusch, F., Tian, L., Tong, A.-M., Gu, J.-Q., Jiang, W., Lu, Z.-T., Shao, L., Tang, M.-X., Yang, G.-M., Zhang, M.-J., and Zhao, L.: A Tibetan ice core covering the past 1,300 years radiometrically dated with ³⁹Ar, Proceedings of the National Academy of Sciences, 119, e2200835119, 2022.

Schwander, J., Stauffer, B., and Sigg, A.: Air mixing in firn and the age of the air at pore close-off, Annals of Glaciology, 10, 141-145, 1988.

Sigl, M., Jenk, T. M., Kellerhals, T., Szidat, S., Gäggeler, H. W., Wacker, L., Synal, H. A., Boutron, C., Barbante, C., Gabrieli, J., and Schwikowski, M.: Towards radiocarbon dating of ice cores, Journal of Glaciology, 55, 985-996, 2009.

Wachs, D., Spagnesi, A., Bohleber, P., Fischer, A., Stocker-Waldhuber, M., Junkermann, A., Kindermann, C., Langenbacher, L., Mandaric, N., Marks, J., Meienburg, F., Jenk, T. M., Oberthaler, M. K., and Aeschbach, W.: A continuous 6000 a age depth relationship for the remainder of the Weißseespitze summit glacier based on 39Ar and 14C dating, Clim. Past, 22, 173-185, 2026.